Resilient Cities and Structures 5 (2026) 1–19

Contents lists available at ScienceDirect

Resilient Cities and Structures

journal homepage: www.elsevier.com/locate/rcns

Full Length Article

A taxonomy-based rapid assessment procedure for seismic risk classification of single-story precast RC buildings

Marius Eteme Minkada, Andrea Belleri *, Marco Bosio, Luca Rota

University of Bergamo, Department of Engineering and Applied Sciences, Dalmine, Italy

ARTICLE INFO

Keywords:
Precast industrial buildings
Seismic risk assessment
Non-structural components
Fragility curves
Building content

ABSTRACT

Past earthquake-related events have highlighted the vulnerability of Italian precast buildings, which are widely used for industrial purposes and therefore represent a significant source of potential economic loss in the event of an earthquake. In this context, insurance companies play a decisive role in the financial protection against earthquake-induced damage, and rapid and reliable procedures for seismic risk classification are essential for the preliminary definition of suitable policies. This study presents a taxonomy-based rapid assessment procedure for the seismic risk classification of single-storey precast reinforced concrete (RC) buildings. The approach introduces a classification framework that correlates building characteristics, construction period and seismic code evolution with corresponding fragility and demand models.

By integrating fragility functions for structural elements, non-structural components and operational content (such as plant and machinery), the method enables a multi-component damage assessment leading to damage-based risk classes. The method was developed considering five representative building classes categorized based on their construction period and seismic regulations. The approach was validated using a case study of a RC precast building damaged during the 2012 Emilia earthquake, for which the main characteristics of the seismic event and the observed damage distribution are considered. This showed a strong correlation between the estimated and observed damage states, confirming the ability of the procedure to capture the main sources of structural and non-structural vulnerability. The proposed methodology provides a practical and transparent tool for large-scale screening and preliminary decision-making and is well suited for implementation in user-oriented software tools that allow even non-experts to assess the seismic classification of single-story precast industrial buildings built in Italy from the post-war period to the present day.

1. Introduction

Assessing the seismic risk of structures is a fundamental step in ensuring the safety of buildings and protecting human life. According to ISO 31010 [1], risk is defined as the combination of the probability of an event and its consequences. For seismic events, risk results from the interaction between hazard, exposure and vulnerability. While seismic hazard and exposure are largely shaped by geographic and urban characteristics, reducing vulnerability remains the most feasible and effective strategy to mitigate seismic risk. In this study, the focus is placed on the vulnerability component of seismic risk, which is used as the basis for a simplified risk classification approach. This includes not only structural retrofitting, but also the implementation of effective methods to assess and prioritize measures based on the level of risk [2]. In this context, simplified assessment methods and visual screening approaches have become important tools for risk prioritization, especially when detailed data is lacking, or rapid assessments are required. Techniques such as Damage Probability Matrices (DPM), observational fragility curves from observations and expert judgment-based scoring systems focus on the use of minimal but important data such as building typology, year of construction and geographical location to estimate vulnerability [3–6]. These methods provide practical and scalable solutions for identifying the most vulnerable structures in large building populations. Similarly, visual screening methods provide a rapid initial assessment by evaluating structural features and environmental conditions, often using standardized checklists or predefined scoring systems. Tools such as NODE [7] further develop this approach by automating the calculation of nominal risk indices, enabling rapid and quantitative prioritization of buildings that require more in-depth analysis.

At the other end, advanced tools such as GIS-based mapping and

* Corresponding author.
E-mail address: andrea.belleri@unibg.it (A. Belleri).

https://doi.org/10.1016/j.rcns.2026.04.005
Received 6 November 2025; Received in revised form 25 March 2026; Accepted 24 April 2026
Available online 9 May 2026

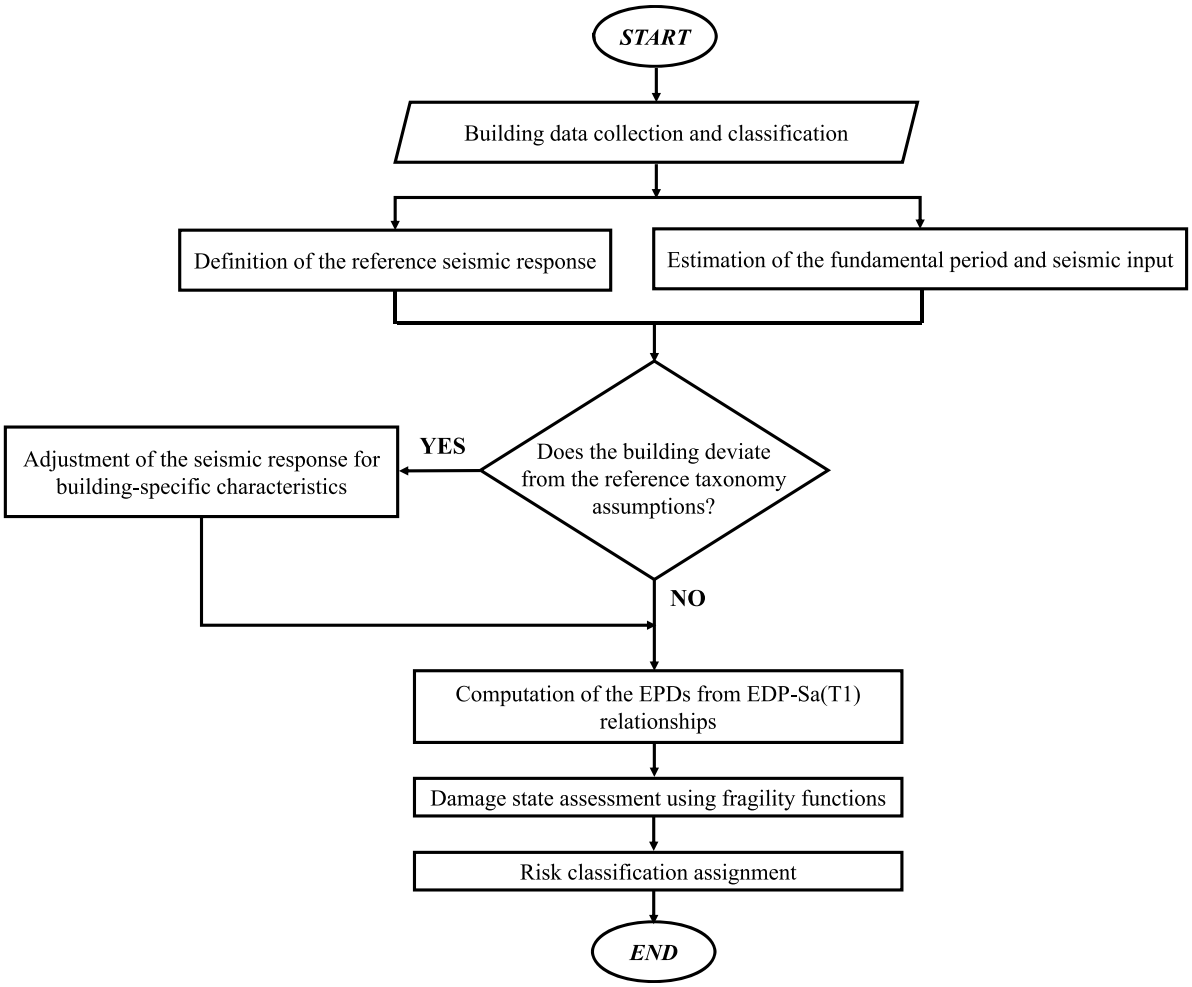

Fig. 1. Flowchart of the proposed taxonomy-based seismic risk classification procedure.

multi-criteria decision making (MCDM) techniques support more comprehensive assessments. These systems integrate a wide range of variables, from regional vulnerabilities to exposure scenarios, to provide a more nuanced understanding of seismic risk at a territorial scale [8–11]. More recently, hybrid approaches combining nonlinear structural analyses and machine learning techniques have been proposed to efficiently predict seismic vulnerability with high accuracy, offering an effective compromise between analytical depth and computational speed [12]. Although they provide deeper insights, their implementation often requires considerable resources and expertise, making them particularly suitable for targeted applications or as second-level assessments after an initial screening. Despite these advances, there is still a need for transparent and mechanically interpretable simplified procedures that can bridge the gap between large-scale screening methods and detailed analytical approaches.

The use of precast construction in industrial and commercial buildings became widespread in Italy in the mid-20th century, as in much of Europe. As a result, a large proportion of these buildings were designed and built without applying modern seismic design criteria. The seismic events that occurred in Emilia in 2012 have caused extensive damage to precast buildings and highlighted their inherent vulnerability [13–22]. The observed damage mechanisms, often associated with connection failures and inadequate detailing, have been widely documented and represent a key aspect in the seismic performance of these structures. The affected area was very large and densely populated, with numerous industrial and commercial settlements. For context, it should be noted that the structural damage involved approximately 15,000 public and healthcare buildings, >14,000 residential buildings, and around 13,000 economic establishments, including industrial, commercial, agricultural facilities, shops, and offices. Regarding the economic impact, the damage in the Emilia-Romagna region alone was estimated at over €12.2 billion [23]. It is noteworthy that the observed damage affected not only older buildings, but also some newer buildings. In this context, researchers have made considerable efforts over the last decade to assess the seismic vulnerabilities and risks of both existing [24–27] and code-compliant precast industrial buildings [19,28,29]. These studies provide valuable fragility models and analytical insights, which constitute a relevant basis for simplified assessment approaches.

Some of the research results available in the literature are summarized below. Bosio et al. [27] pointed out the high seismic risk of prefabricated industrial buildings constructed in the 1960s-1970s and 1980s-1990s. Other researchers [24,25] have focused on the assessment of the seismic performance of precast RC buildings designed according to the current Italian building code [26], showing a low seismic risk with a demand-to-capacity ratio well below code limits for both structural elements and connections. However, these studies are typically based on detailed numerical modelling and are not directly suitable for rapid large-scale applications. In general, previous studies have often addressed the seismic performance of individual structural components without comprehensively considering the contribution of non-structural elements and operational contents (e.g. equipment and machinery). From a risk-oriented perspective, this represents a significant limitation, as in industrial buildings the value of contents often exceeds that of the structural system itself. Several studies have confirmed the sensitivity of

industrial facilities to dynamic actions. Including these elements in a seismic assessment framework would allow a more comprehensive evaluation of potential losses.

The main objective of this article is to propose taxonomy-based procedure for the rapid seismic risk classification of typical single-storey precast industrial buildings, considering both structural and non-structural components as well as operational contents. Five building classes are defined, reflecting the main periods of change in the evolution of Italian seismic regulations from the post-war period to the present day. For each class, a reference structural configuration is adopted to derive baseline seismic response models, intended as representative archetypes for the considered taxonomy. The baseline seismic response for each building class was derived by multi-stripe analyses on simplified 2D models, while parametric analyses based on more refined 3D numerical were performed to evaluate the influence of specific features, such as cladding systems or plan and elevation irregularities. Based on these analyses, correction factors are introduced to update the Engineering Demand Parameter (EDP) curves, which describe the seismic response of each building class. The damage state of each component (structural, non-structural and contents) is evaluated by combining EDP-based demand estimates with component-specific fragility functions. The final outcome of the procedure is expressed in terms of damage-based risk classes, defined consistently with limit state exceedance (e.g. Damage Limit and Life Safety) and intended for comparative assessment and decision-making purposes. The proposed method was validated using a case study of a precast RC building damaged during the 2012 Emilia earthquake. The characteristics of the seismic event and the observed damage patterns are explicitly considered to assess the consistency between predicted and observed damage. In addition to this validation, the procedure is tested under seismic scenarios corresponding to the Damage Limit (DL) and Life Safety (LS) performance levels, in order to evaluate its capability to differentiate between different seismic intensity levels.

2. Proposed procedure

This section first provides a general overview of the proposed methodology and describes the criteria adopted for damage assessment and risk classification. The procedure is conceived as a taxonomy-based framework that combines simplified structural modelling with component-level fragility functions to enable a rapid and transparent damage-based seismic risk classification. Fig. 1 shows an overview of the proposed workflow. The process consists of seven key steps, ranging from data collection to risk classification, each associated with clearly defined inputs, computational procedures, and outputs, as described below.

Step 1. Data collection and building classification. Relevant building information is collected, including location, year of construction, height and any available data on previous retrofit measures. The building is classified into one of five taxonomy classes, and the corresponding baseline EDP-Sa(T_1) curves are selected. In addition, specific building characteristics are recorded, as these parameters are crucial for refining the demand estimation.

Step 2. Definition of the reference seismic response. A set of EDP-Sa(T_1) relationships is defined to represent the baseline seismic response of each taxonomy class, where Sa(T_1) is the spectral ordinate at the fundamental vibration period of the building (T_1). These relationships are derived from analyses on reference structural configurations (archetypes), intended as baseline representations of recurring structural features rather than exhaustive descriptions of the building stock, and provide a simplified but mechanically consistent link between seismic intensity and structural demand.

Step 3. Estimation of the fundamental period and seismic input. In this phase, the fundamental vibration period of the building is estimated using simplified analytical expressions based on structural typology and the expected seismic action in the form of spectral accelerations is determined on the basis of the building site.

Step 4. Adjustment of the seismic response for building-specific characteristics. The reference EDP-Sa(T_1) curves established in Step 2 are updated based on the specific characteristics of the building. This adjustment is performed through correction factors derived from parametric analyses on refined 3D numerical models, explicitly accounting for key sources of variability such as cladding typology, plan irregularities, connection behaviour and panel–structure interaction mechanisms.

Step 5. Computation of the building's seismic response. The relevant EDP values for the examined building are obtained by combining the site-specific spectral acceleration with the class-specific, and where needed corrected, EDP-Sa(T_1) relationships.

Step 6. Damage state assessment. The specific EDP values determined in Step 5 are used to determine the damage state of each element (structural, non-structural and contents). This is performed through component-specific fragility functions, which provide the probability of exceeding each damage state as a function of the corresponding EDP. In practice, the damage state is assigned based on a probability threshold of 50 %, which is adopted as a reference value but can be adjusted depending on the desired level of conservatism. The applicability of this step depends on the availability of fragility functions for the considered components.

Step 7. Risk classification assignment. In this step, damage-based risk classes are assigned based on the damage states established in Step 6, following the criteria outlined in Section 2.2. The resulting classification is intended for comparative assessment and prioritization rather than for direct loss quantification.

Beyond its operational workflow, the proposed seven-step framework is conceptually consistent with the classical definition of seismic risk as the interaction between hazard, exposure, and vulnerability. However, it should be emphasized that the present procedure primarily focuses on the vulnerability component, which is used as the basis for the definition of damage-based risk classes. The hazard is represented by the site-specific spectral acceleration Sa(T_1), while vulnerability is captured through fragility functions relating engineering demand parameters to damage probabilities. Exposure is only partially represented through the inclusion of operational contents, without explicit modelling of economic value or loss consequences. Therefore, the proposed approach should be interpreted as a vulnerability-driven, risk-oriented classification framework rather than a complete probabilistic risk assessment. A full probabilistic risk assessment would require the explicit integration of exposure and consequence models, which is beyond the scope of the present study.

Regarding the fragility functions developed in this study (Section 4), it is important to position the proposed approach within the broader context of available fragility datasets. Existing frameworks such as HAZUS [30] and GEM [31] provide comprehensive fragility models for conventional structural typologies. However, their applicability to single-storey precast industrial buildings is limited, particularly with respect to interaction mechanisms between non-structural components, connections, and the supporting structure, which are key drivers of seismic vulnerability in these systems. For this reason, the present study adopts and further develops fragility functions specifically calibrated for taxonomy-based classes of precast industrial buildings, derived from nonlinear analyses and including both structural and non-structural components.

2.1. Damage assessment and risk classification

In the proposed procedure, damage assessment is performed through component-specific fragility functions that relate selected EDP to the probability of exceeding predefined damage states. Within a performance-based framework, these functions enable the correlation of

Table 1
Fragility parameters for displacement-sensitive components (lognormal distribution; θ expressed as median drift or relative displacement).

θ = median drift over height of the building										
	DS1		DS2		DS3		DS4		DS5	
Element	θ	β	θ	β	θ	β	θ	β	θ	β
Column 1	0.0150	0.40	0.0180	0.40	0.0210	0.40	0.0438	0.40	-	-
Column 2	0.0192	0.40	0.0292	0.40	0.0392	0.40	0.0660	0.40	-	-
Column 3	0.0200	0.40	0.0290	0.40	0.0380	0.40	0.0680	0.40	-	-
Masonry infills	0.0018	0.52	0.0046	0.54	0.0105	0.40	0.0188	0.38	-	-
Windows	0.0060	0.12	0.0096	0.25	0.0110	0.20	0.0160	0.19	0.02	0.16
Drywall partitions	0.0021	0.58	0.0065	0.43	0.0116	0.45	-	-	-	-
Internal doors	0.0023	0.90	0.0056	0.40	-	-	-	-	-	-
θ = relative displacement of the connection element										
	DS1		DS2		DS3		DS4		DS5	
Element	θ	β	θ	β	θ	β	θ	β	θ	β
Roof element	0.0050	0.40	0.0100	0.40	0.0200	0.40	0.0400	0.40	0.06	0.40
Sealant	0.0048	0.15	0.0096	0.25	-	-	-	-	-	-
Vertical panels 1	-	-	-	-	0.0600	0.40	0.0700	0.40	-	-
Vertical panels 2	-	-	-	-	0.0600	0.40	0.2000	0.40	-	-
Horizontal panels	-	-	-	-	0.0400	0.40	0.0500	0.40	-	-

Table 2
Fragility parameters for acceleration-sensitive components (lognormal distribution, values in g).

Element	DS1		DS2		Element	DS1		DS2	
	θ	β	θ	β		θ	β	θ	β
Storage racks	0.42	0.43	0.43	0.29	Generator	1.30	0.60	-	-
Overhead crane	-	-	0.25	0.30	Electrical panel	1.20	0.60		
Hydraulic elevator	0.41	0.30			Control centre	1.80	0.60	-	-
Electric elevator	0.35	0.06	-	-	Compressor	0.90	0.60	-	-
	0.35	0.17							
Refrigerator	0.64	0.40	-	-	Air handling unit	1.50	0.60	-	-
Distribution panel	3.40	0.60	-	-	Cooling towers	1.20	0.40	-	-

seismic intensity with structural damage, allowing the damage state of each element to be associated with the attainment of specific EDP thresholds such as interstorey drift ratio or absolute acceleration. Overall, this leads to a probabilistic damage assessment approach in which each possible damage state (DS) of an element is represented by a fragility curve that relates a significant EDP to the probability of exceeding that damage state.

The fragility curves used in this paper follow a lognormal distribution (Eq. 1):

$$F_X(x) = P[\mathrm{DS} \geq DS_i | \mathrm{EDP} = x] = \Phi\left(\frac{\ln x - \theta}{\beta}\right) \quad (1)$$

Where θ and β are parameters representing the mean and standard deviation of the logarithmic values, respectively, Φ is the cumulative distribution function of the normal distribution and $P[\mathrm{DS} \geq DS_i \mid \mathrm{EDP} = x]$ represents the probability that a component will experience a damage state (DS) equal to or greater than DS_i, after being subjected to an EDP equal to x.

For structural elements such as columns and roof components, the fragility curve parameters were derived from recent studies [28,32]. For non-structural elements and building contents, the fragility curves from FEMA P-58 [33] were adopted.

The procedure is formulated in a modular way and can be extended to additional components, provided that appropriate fragility functions are available.

The set of elements considered in this study, although not exhaustive, is intended to represent typical components commonly found in industrial precast buildings.

The fragility parameters adopted for the selected components are summarised in Tables 1 and Table 2, grouped according to the type of EDP, namely displacement-sensitive and acceleration-sensitive components. For displacement-sensitive elements (Table 1), the parameter θ represents either the median interstorey drift ratio, computed with respect to the building height (H), or the relative displacement between connected elements. In the latter case, the reference element is specified in the corresponding column. In this study, the building height (H) is defined as the clear height under the beam.

Different fragility models are introduced to account for variations in

Table 3
Definition of intrinsic seismic risk classes according to the macroseismic intensity scale.

Perceived shaking [-]	Potential damage [-]	Peak acceleration [%g]	Peak velocity [cm/s]	Instrumental intensity [-]	Considered seismic risk class [-]
Not felt	None	< 0.06	< 0.02	I	C0
Weak	None	0.2	0.08	II-III	C0
Light	None	0.8	0.3	IV	C1
Moderate	Very light	2	0.9	V	C2
Strong	light	4.8	2.4	VI	C2
Very strong	Moderate	12	6.4	VII	C3
Severe	Moderate/ Heavy	29	17	VIII	C4
Violent	Heavy	70	45	IX	C5
Extreme	Very heavy	> 171	> 120	X+	C5

Table 4
Assignment of risk classes to structural and non-structural components based on damage states.

Element	DS1	DS2	DS3	DS4	DS5
Column	C2	C3	C4	C5	-
Roof element	C2	C2	C3	C4	C5
Sealant	C1	C2	-	-	-
Vertical panel	-	-	C2	C3	-
Horizontal panel	-	-	C2	C3	-
Masonry infill	C1	C1	C2	C3	-
Windows	C1	C2	C2	C2	C3
Drywall partition	C1	C2	C2	-	-
Internal door	C2	C2	-	-	-

Table 5
Assignment of risk classes to content-related components.

Element	DS1	DS2	Element	DS1	DS2
Storage racks	C2	C3	Generator	C3	-
Overhead crane	C2	C3	Electrical panel	C2	-
Hydraulic elevator	C3	-	Control centre	C2	-
Electric elevator	C3	-	Air compressor	C2	-
Refrigerator	C2	-	Air handling unit	C2	-
Distribution panel	C2	-	Cooling towers	C2	-

structural typologies across construction periods. Three types of column fragility curves are considered: Column 1 refers to buildings constructed up to 2003, while Column 2 and Column 3 correspond to post-2003 buildings with low and high dissipation capacity, respectively. Similarly, Vertical Panel 1 and Vertical Panel 2 represent cladding systems associated with pre- and post-2003 construction practices.

The seismic risk classes, based on the macroseismic intensity scale (Table 3), are defined by grouping seismic intensity ranges into discrete classes (C0-C5) and are subsequently applied to the elements as summarised in Tables 4 and Table 5. The assignment of risk classes to individual elements is performed by linking component-level damage states to expected global damage scenarios, using the EMS-98 scale [34] as a reference framework. For example, limited damage in a column characterised by small cracks (DS2) corresponds to a 'moderate' global damage scenario, to which risk class C3 is assigned, while collapse (DS4) is associated with risk class C5. Detailed descriptions of the adopted damage states and the corresponding mapping criteria are provided in Appendix A.

The proposed classification is intended to provide a consistent and traceable ranking of expected damage severity, rather than a precise quantitative estimate of economic loss. The mapping between component damage states and risk classes is established based on their correspondence with macroseismic damage descriptions, ensuring coherence between local damage and global damage scenarios. Although this approach involves an element of expert judgement, it enables a rational and transparent link between seismic intensity, damage states, and the resulting risk classification.

3. Taxonomy-based classification framework for precast industrial buildings

A taxonomy-based framework is adopted to classify single-storey precast industrial buildings in Italy according to their main structural characteristics and construction period. Five reference building classes are defined to represent recurring structural configurations observed in practice and to provide a consistent basis for deriving simplified seismic response models. Since this study focuses on the seismic behaviour of these structures, it is essential to analyse the evolution of seismic regulation in Italy, which have directly influenced design practices, connection typologies, and overall structural performance.

3.1. Evolution of seismic regulation in Italy

The consideration of seismic aspects in Italian building codes is often associated with guidelines for use in earthquake-prone areas, published after each major earthquake. Early regulations mainly addressed geometric and prescriptive requirements, such as minimum member dimensions and building height limits, without a fully developed dynamic framework.

Seismic loads were officially included in the regulations in 1916 [35], supplementing the provisions of Decree 193 of April 18, 1909 [36], which was issued after the earthquakes of December 28, 1908, in Calabria and Messina. Decree 193 required the consideration of horizontal and vertical static forces proportional to the weight of the structure, using a predetermined coefficient. In the 1920s, after the earthquakes in Ancona, Perugia, Siena and Grosseto, the legislation was updated [37] and the first seismic zoning system in Italy was introduced.

Over the years, the Italian system for classifying earthquakes has been revised several times. The culmination was Ministerial Decree 3274 [38] which classified the entire Italian territory as earthquake-prone and divided it into four seismic zones. This marked a fundamental shift, as seismic design became mandatory for all new constructions nationwide. Subsequent regulations, such as NTC08 [39] and the current NTC18 [40], further refined the definition of seismic input mainly through updated hazard models developed by the Italian Institute of Geophysics and Volcanology (INGV).

The seismic behaviour of precast buildings is strongly influenced by the characteristics of the structural connections. These buildings are typically frame structures with hinged connections. In 1986 [41] it was established that the use of friction connections must be justified by a specific study, and in 1987 [42], the use of simple friction joints was prohibited in seismic areas. However, in practice, the transition from friction-based to mechanical connections occurred progressively during the 1980s, influenced by both regulatory updates and evolving design practices.

Considering the seismic classification of the entire Italian territory, it can be assumed that structures built since 2003 are generally equipped with mechanical connections. The importance of connection systems in precast buildings was highlighted by the seismic events that struck the Emilia-Romagna region in 2012 [14–17], where the main damage mechanisms were associated with the loss of support and collapse of the roof elements. These observations confirmed the critical role of connection behaviour in governing the seismic vulnerability of this structural typology. Numerous studies have focused on friction joints [24,26, 43–47], while other research has investigated mechanical connections, in particular dowel connections [48–50]. In addition to connection-related vulnerabilities, precast industrial buildings exhibit significant vulnerabilities in masonry infill, cladding systems and columns [13,51–53]. This evolution directly motivates the definition of the taxonomy classes adopted in this study.

3.2. Definition of taxonomy-based reference building classes

The analysis of the evolution of seismic regulations allows the identification of three main periods: before 1984, between 1984 and 2003 and after 2003. Before 1984, there were no significant differences in the design between seismic and non-seismic regions, and precast elements were generally connected using friction joints, often with neoprene layers [43,44]. Between 1984 and 2003, design practices diverged between seismic and non-seismic regions. In seismic areas, mechanical connections became increasingly adopted, while in non-seismic regions friction connections were still commonly used. Since 2003, following the classification of the entire national territory as seismic, mechanical connections became standard practice, and the design framework explicitly introduced the concept of energy dissipation, allowing structures to be designed as non-dissipative (ND) or dissipative (D).

Table 6
Definition of the taxonomy-based reference building classes.

Time period	Site seismicity	Main characteristics	Building class id
Before 1984	Unclassified	Friction connections	Pre-84
1984 - 2003	Non-seismic (NS)	Friction connections	84-NS
	Seismic (S)	Mechanical connections	84-S
From 2003	Seismic (S)	Mechanical connections and non-dissipative design	2003-ND
		Mechanical connections and dissipative design	2003-D

Based on these considerations, five taxonomy-based reference building classes are defined (Table 6). It is emphasized that these classes are not intended to represent the full variability of the existing building stock, but rather to serve as reference archetypes capturing the most recurrent structural configurations within each construction period.

Although the formal prohibition of friction connections in seismic zones was introduced with DM 3/12/1987 [42], the mid-1980s already marked a practical transition in design practice. Following the 1980 Irpinia earthquake and the update of the national seismic classification in 1984, many precast manufacturers progressively abandoned friction joints in seismic regions. For this reason, 1984 is adopted as a reference threshold year for defining the taxonomy classes, reflecting practical design evolution rather than strictly regulatory milestones. Nevertheless, the methodology allows users to directly select the appropriate reference class if the actual connection typology of the building is known, independently of the construction year.

As already mentioned, a reference building must be selected in Step 1 from the classes listed in Table 6. However, any previous retrofit measures affecting the building must also be considered, as they may significantly modify the expected seismic response [31,54,55]. In this context, the selected reference class should be interpreted as a baseline configuration, which can be updated to reflect the actual structural condition of the building. Therefore, the reference building must be determined according to the framework shown in Fig. 2. Starting from Pre-84 or 84-NS buildings, the reference class is updated to 84-S if local retrofit interventions affecting connections have been carried out. In the case of global retrofit, the building is associated with post-2003 classes (2003-ND or 2003-D), depending on the seismic design approach adopted. A similar consideration applies to the reference building class 84-S.

3.3. Calculation of the fundamental period

Once the reference building has been selected, a crucial step is to determine the seismic input in terms of spectral acceleration acting on the building. This assessment is strongly influenced by the modal behaviour of the building, particularly its fundamental period of vibration (T_1). For the considered structural typology, characterized by single-storey frames, the fundamental period can be reasonably estimated using simplified analytical formulations based on geometric properties. Given the design acceleration spectrum for the site, knowledge of T_1 allows the immediate determination of the spectral acceleration $Sa(T_1)$, which directly affects the estimated seismic demand and, consequently, the vulnerability assessment.

The fundamental period of the considered structural typology depends primarily on the roof mass and the stiffness of the columns. Since these parameters vary with construction period and seismic design practices, estimating T_1 for existing buildings may be uncertain. Various formulations have been proposed in the literature; in this study, the expression in Eq. (2) [56] is adopted, as it is specifically calibrated for precast buildings.

$$T_1 = \alpha \cdot H^{3/5} \tag{2}$$

Where H is expressed in meters.

In the proposed approach, the coefficient α is used to account for differences in structural stiffness associated with construction period and seismic design level. For buildings constructed after 2003, α varies depending on the seismic zone, while for earlier buildings a constant value $\alpha = 0.45$ is adopted. Table 7 reports the adopted values. As anticipated in Section 2, the building height (H) is defined as the clear height measured from the top of the floor slab to the underside of the beam.

4. Derivation of $Sa(T_1)$-EDP reference curves and modelling framework

This section describes the derivation of the $Sa(T_1)$-EDP reference curves, which are used to represent the seismic response of the taxonomy-based reference buildings introduced in Section 3. The objective is to define simplified yet mechanically consistent relationships between seismic intensity and EDPs, suitable for rapid assessment procedures. A representative structural configuration is adopted as a reference archetype, reflecting recurrent geometric and structural features of single-storey precast industrial buildings in Italy, as documented in previous studies [27]. While not intended to capture the full variability of the existing building stock, this configuration provides a consistent basis for comparative analyses and for the development of

Table 7
α values for estimating the building's fundamental period according to Eq. (2).

Construction Period	Seismic region	α [-]
After 2003	I	0.25
	II	0.28
	III	0.31
	IV	0.36
Before 2003	-	0.45

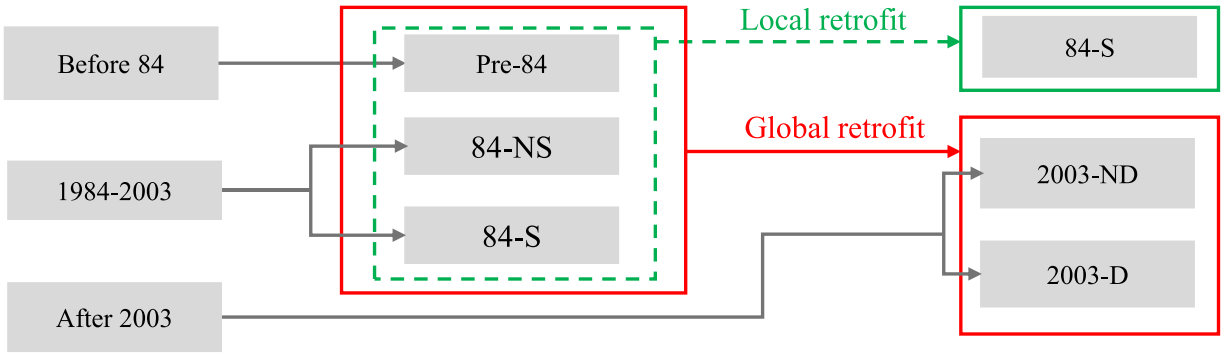

Fig. 2. Framework for the selection and updating of the reference building class.

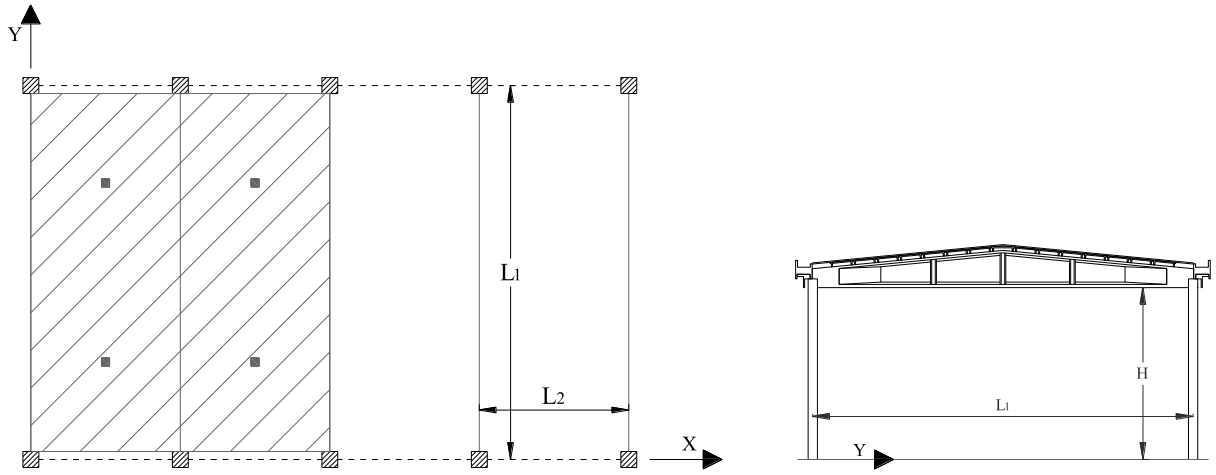

Fig. 3. Reference structural geometry adopted for the derivation of baseline response models: plan view with mezzanine position (left) and transverse section (right).

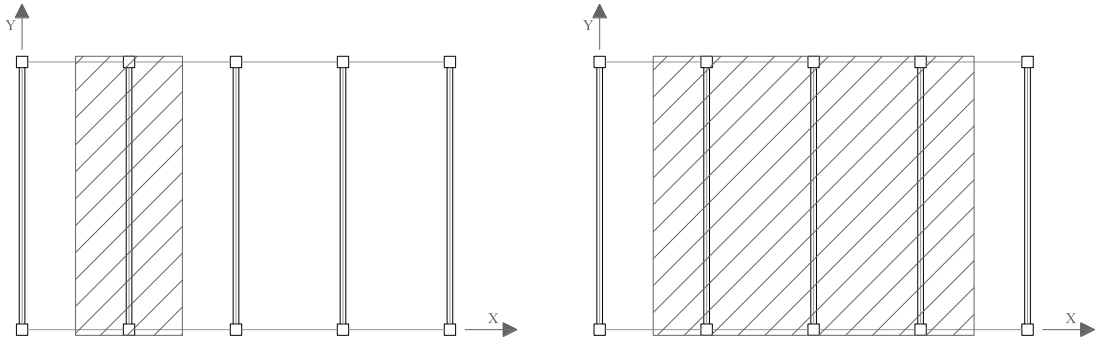

. 4. Tributary areas considered for the simplified models: Model 1(left) and Model 2 (right).

simplified seismic demand models within the proposed framework.

The adopted geometry (Fig. 3) consists of a series of portal frames composed of two columns and a double-slope beam supporting precast roof elements. The beam length (L_1), frame spacing (L_2), and clear height (H) are assumed equal to 20 m, 6 m, and 7 m, respectively. Similar geometric assumptions are consistent with previous studies [27], while material properties and connection details are defined consistently with the adopted modelling framework.

4.1. Simplified numerical modelling approach

The seismic response of the base buildings was evaluated through nonlinear multi-stripe analyses using simplified two-dimensional models in OpenSees [58]. The modelling strategy is aimed at capturing the dominant nonlinear mechanisms governing the seismic behaviour of precast structures, while maintaining computational efficiency suitable for parametric analyses. Two simplified 2D models were adopted to represent the structural response of the building in the transverse (Model 1) and longitudinal (Model 2) directions, as shown in Fig. 5.

- Model 1 (Fig. 5-left) represents an internal frame of the structure, associated with the tributary area shown in Fig. 4-left. This model consists of two vertical elements (columns) and one horizontal element (beam), modelled with an equivalent constant cross-section.

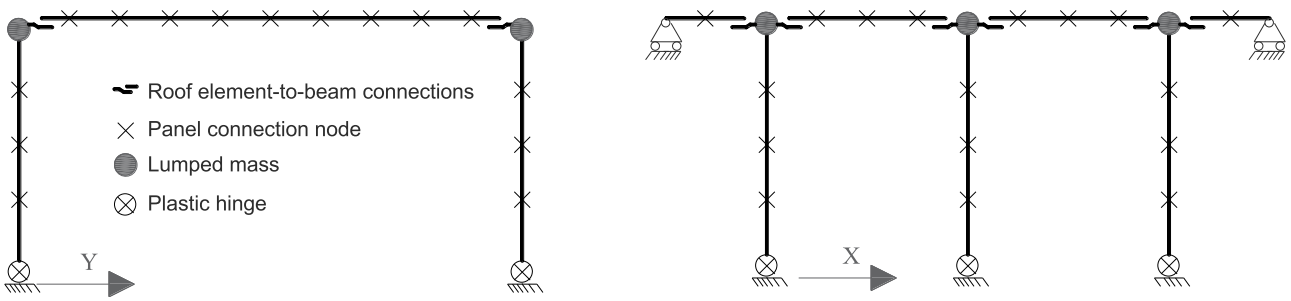

. 5. Simplified 2D modelling schemes for transverse (Model 1, left) and longitudinal (Model 2, right) directions.

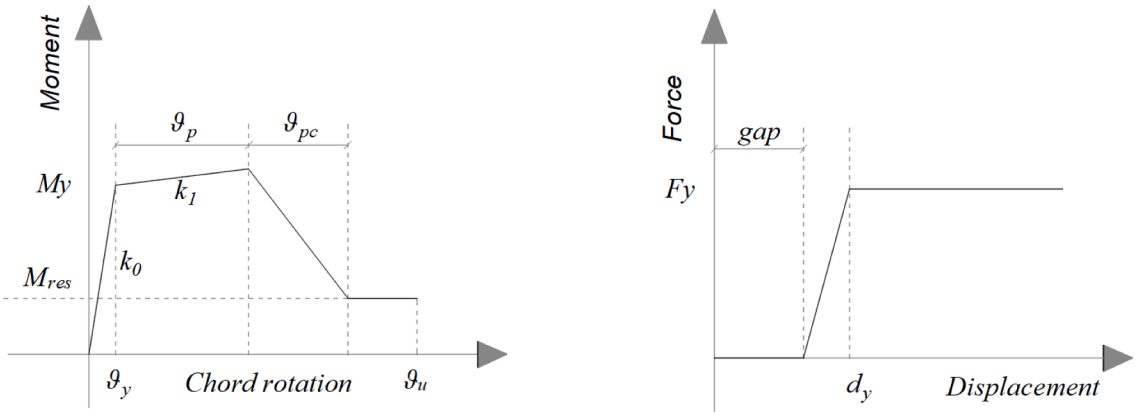

Fig. 6. Hysteretic models adopted for nonlinear components: Modified Ibarra-Medina-Krawinkler model (left) and elastic–perfectly plastic gap material (right). k_0 and M_y denote the initial elastic stiffness and yield moment, respectively; θ_p, θ_{pc}, and θ_u represent the pre-capping, post-capping, and ultimate rotations; F_y and d_y denote the yield force and corresponding displacement.

Table 8
Plastic hinge parameters for reinforced concrete columns used in the reference building models.

	k_0 [kNm/rad]	k_1/k_0 [-]	M_y [kNm]	ϑ_p [rad]	ϑ_{pc} [rad]	ϑ_u [rad]	M_{res} [kNm]
Pre-84	4830	0.212	111	0.026	0.030	0.2	22
84-NS	12,200	0.075	178	0.048	0.035	0.2	36
84-S	43,100	0.070	263	0.017	0.043	0.2	63
2003-ND	9710	0.270	194	0.018	0.047	0.2	39
2003-D	20,062	0.230	383	0.020	0.043	0.2	77

This simplification is justified by the limited influence of beam slope (typically around 10 - 15 %) on global seismic response.

- Model 2 (Fig. 5-right) represents two adjacent bays with the tributary area shown in Fig. 4-right. This model includes three vertical elements and four horizontal elements, reproducing the mass and stiffness distribution of the longitudinal direction.

Beams and roof elements are modelled as elastic components, assuming that their contribution to nonlinear behaviour is secondary compared to columns and connections [59]. This assumption is supported by post-earthquake observations, which indicate that seismic damage in precast industrial buildings is mainly governed by plastic hinges at the base of the columns and by the connections between precast elements. RC columns are modelled using a lumped plastic hinge at the base coupled with an elastic element. Cracked stiffness is accounted for by reducing the elastic modulus by 50 %. The nonlinear behaviour is represented using the Modified Ibarra-Medina-Krawinkler model [61], shown in Fig. 6-left, with the characteristics evaluated according to the structural details (Table 8).

Connection behaviour is explicitly considered, as it represents a key source of vulnerability in precast structures. Friction-based beam-to-column connections are modelled using a Flat Slider Bearing element, with a friction coefficient of 0.13 and an initial stiffness of 490 kN/m [27]. Mechanical beam-to-column connections are idealised as pinned joints at the global level, while their seismic performance is evaluated in post-processing based on the corresponding demand parameters. This assumption is consistent with common design practice and allows

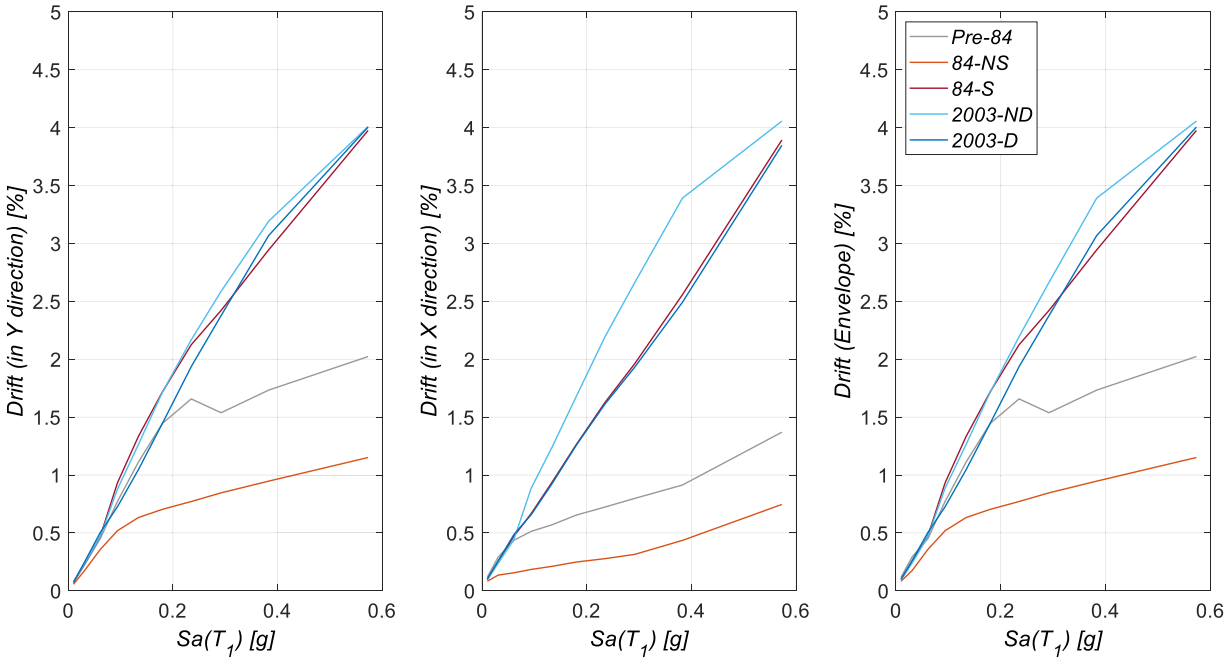

Fig. 7. Sa(T_1)-drift relationships derived from multi-stripe analyses (transverse, longitudinal, and envelope responses).

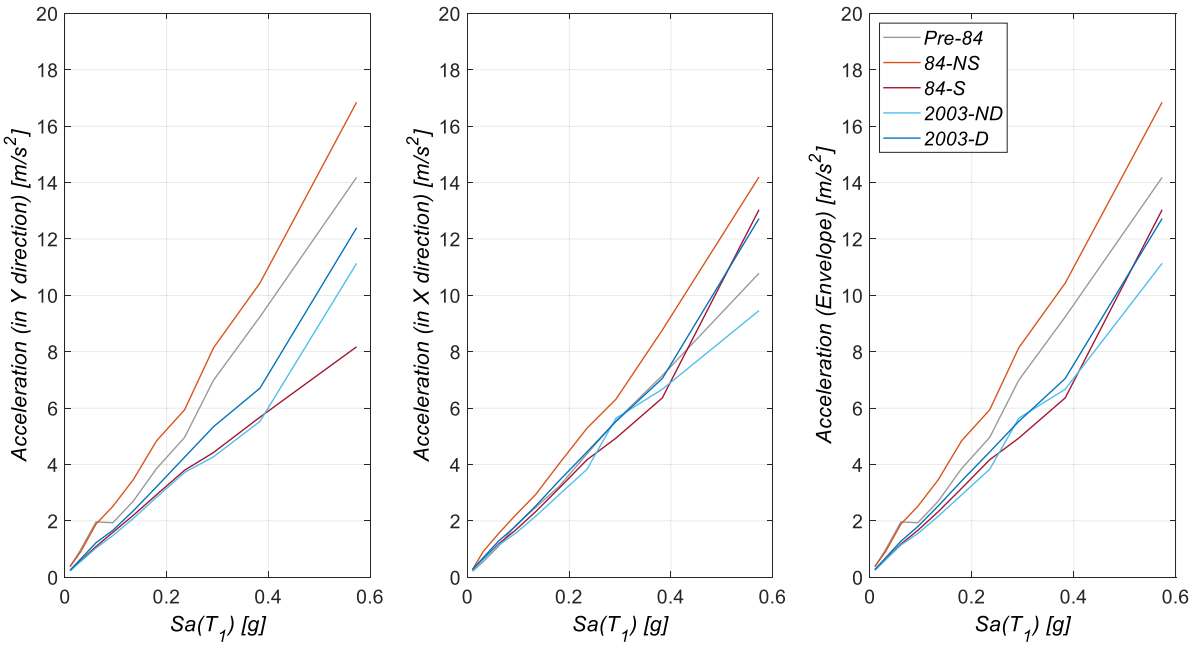

Fig. 8. Sa(T_1)-roof acceleration relationships for the reference buildings.

isolating the influence of connection behaviour on global response, which is subsequently accounted for through component-level fragility functions. Roof connections are modelled consistently with construction period. Friction connections are represented using Flat Slider Bearing elements, while mechanical connections are modelled using Elastic-Plastic hysteretic laws calibrated according to Bressanelli et al. [21]. The adopted modelling strategy aims to capture the dominant behaviour of connection systems rather than their full variability. While connection response may be influenced by several factors (e.g. detailing, degradation, and construction tolerances), these aspects are indirectly accounted for in the fragility-based assessment framework, which incorporates variability at the component level, ensuring consistency with the probabilistic nature of the assessment.

The boundary conditions consist of fixed supports at the base of the columns. For Model 2, additional constraints are applied at the outer ends of the roof elements, allowing rotation and horizontal displacement. A uniform roof load of 5 kN/m^2 is considered, including the contribution of beams and roofing elements.

4.2. Multi-stripe analysis and results

Nonlinear multi-stripe analyses [27,32] were performed using ten intensity levels, selected to cover a wide range of seismic demand consistent with the Italian MPS04 model [62]. The adopted spectral acceleration values Sa(T_1), in g, corresponding to a reference period T_1 = 1.5 s, are equal to 0.010, 0.031, 0.061, 0.094, 0.134, 0.180, 0.235, 0.292, 0.382, and 0.573. For each intensity level, seven ground motion records were selected using the REXEL tool [63], ensuring record-to-record variability. The results of the multi-stripe analyses are expressed in terms of Sa(T_1)-EDP relationships for the considered

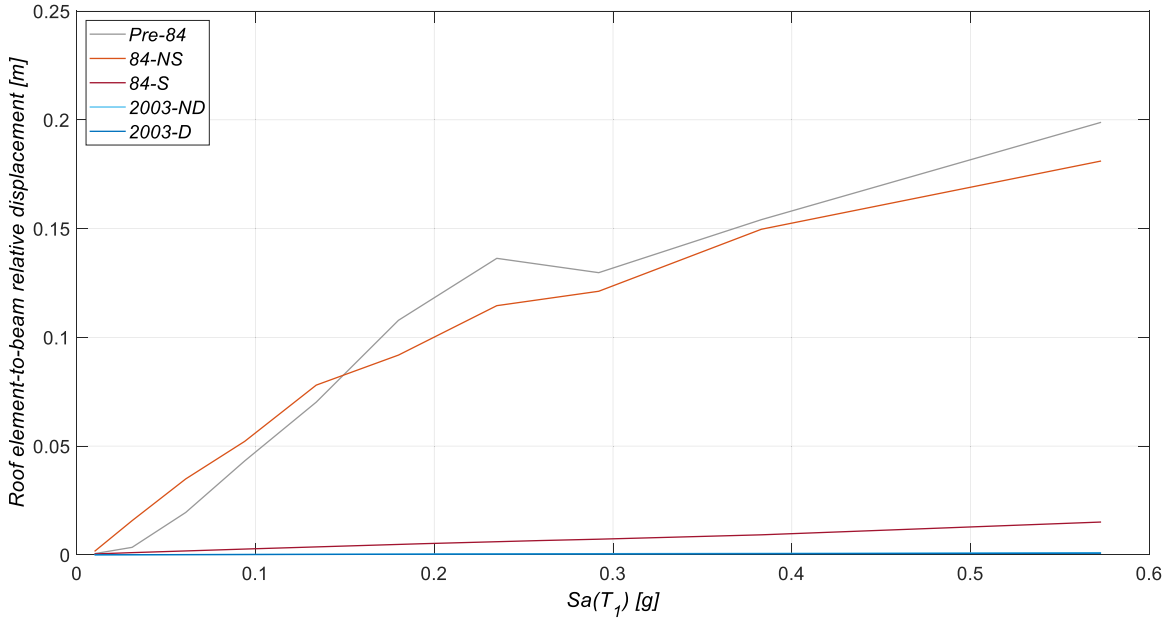

Fig. 9. Relative displacement demand at the roof element-to-beam connections.

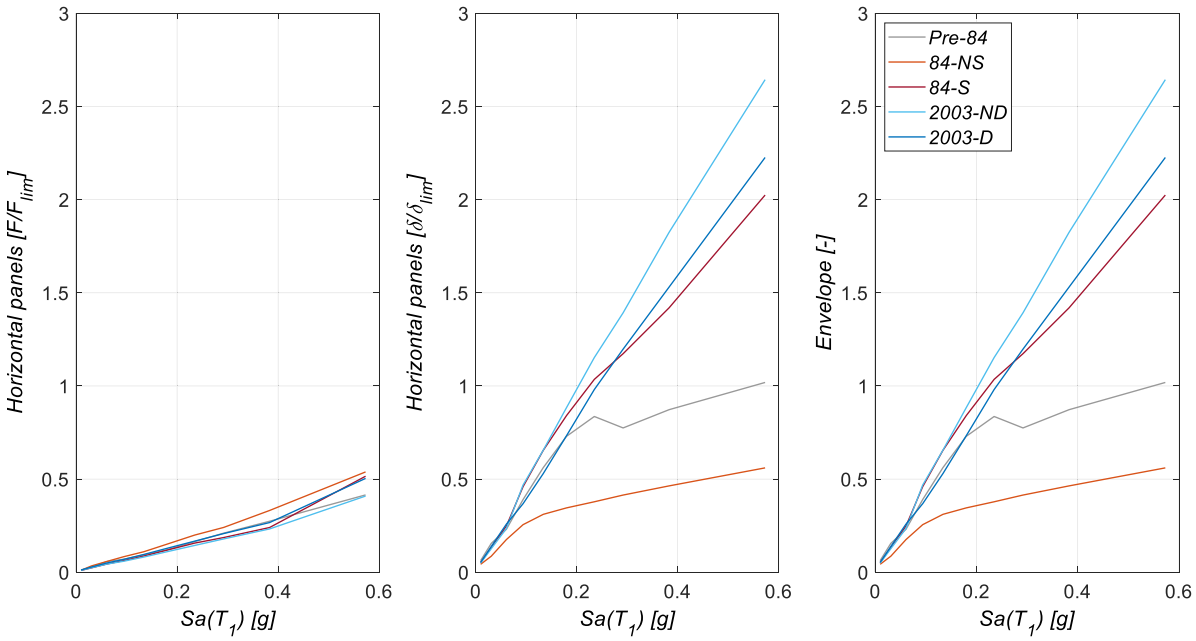

Fig. 10. Dimensionless demand (normalised force and displacement) for horizontal cladding panels.

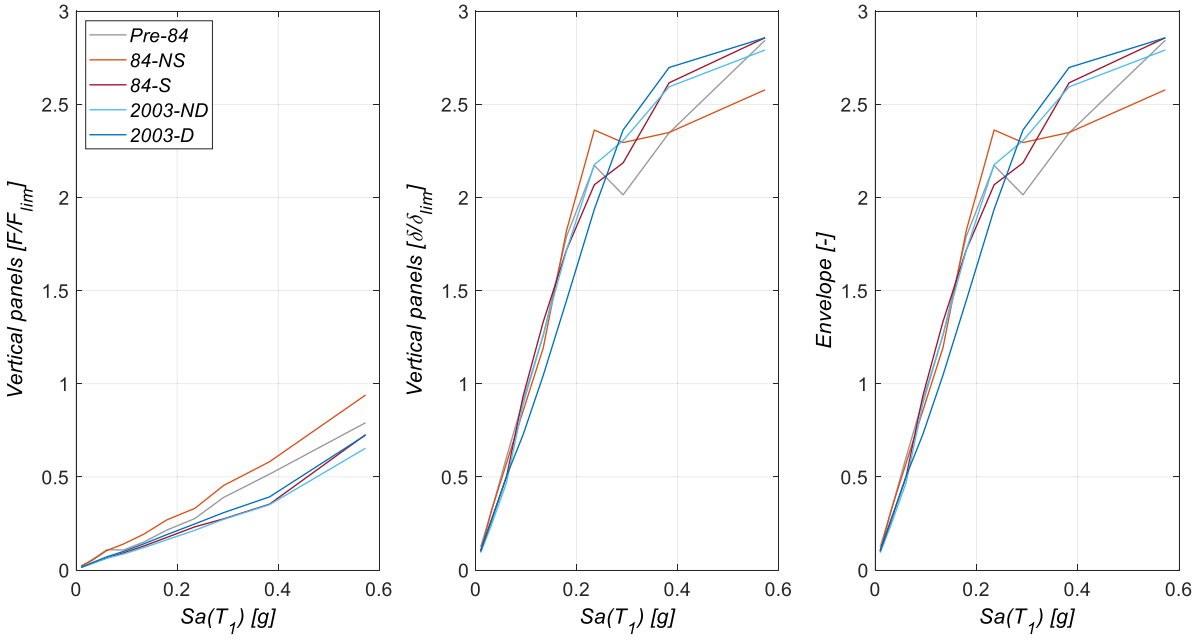

Fig. 11. Dimensionless demand (normalised force and displacement) for vertical cladding panels.

reference buildings. Fig. 7 shows the Sa(T_1)-drift curves. The left plot and middle plots correspond to the transverse (Model 1) and longitudinal (Model 2) directions, respectively, while the right plot shows the envelope of the two. The results indicate a comparable structural response in both directions.

From the envelope curves (Fig. 7-right), it emerges that the "Pre-84″ and "2003-D" buildings exhibit similar drift values up to 0.2 g. Beyond this threshold, the "Pre-84″ building shows a clear deviation from linear behaviour. A similar trend is observed for the "84-S" and "2003-ND" buildings, with the former exhibiting earlier nonlinear response. The "84-NS" building shows significantly lower drift values compared to the other typologies. Notably, the "84-NS" and "Pre-84" buildings exhibit nonlinear behaviour at approximately 0.1 g and 0.2 g, respectively, which can be attributed to the activation of sliding mechanisms in friction-based connections.

Fig. 8 shows the roof acceleration as a function of the spectral acceleration. The results confirm a consistent response in the two principal directions, with acceleration increasing with Sa(T_1). The highest acceleration demands are observed for the "84-NS" and "Pre-84" buildings, indicating a greater sensitivity of older structures to seismic input.

Fig. 9 shows the relative displacement at the roof element-to-beam connections. The results highlight the increased vulnerability of buildings with friction-based connections ("Pre-84″ and "84-NS"), while post-2003 buildings exhibit nearly flat curves, indicating improved seismic performance.

Fig. 10 and Fig. 11 present the demand on cladding panels in terms of out-of-plane force and in-plane relative displacement. Due to the use of a 2D modelling approach, out-of-plane forces are derived from Model 2

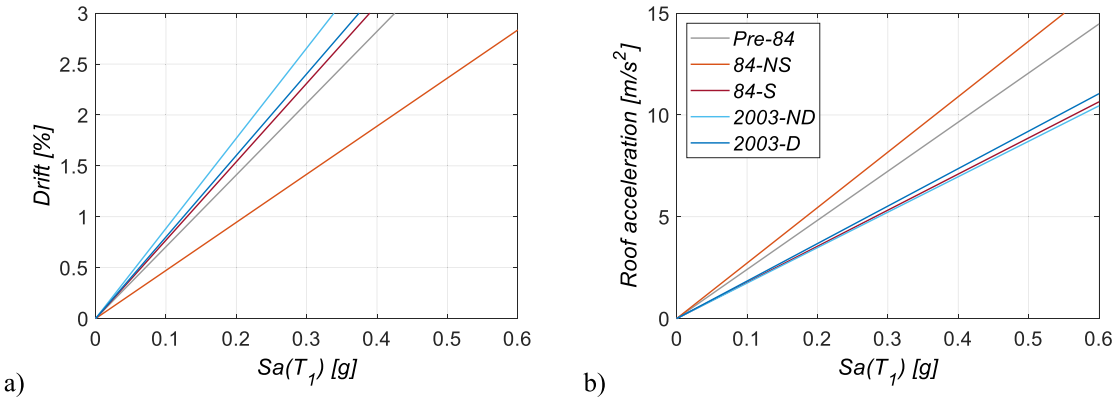

Fig. 12. Examples of linearised Sa(T₁)–EDP relationships: (a) roof displacement and (b) roof acceleration.

when analysing Model 1, and vice versa. To obtain a consistent response envelope, force and displacement demands are normalised with respect to their corresponding design values [28,32]. The results indicate that, for all building typologies, the response envelope is governed by in-plane displacement demand. For horizontal panels (Fig. 10), the trend closely follows the global drift response, whereas for vertical panels (Fig. 11) a different pattern emerges, reflecting their distinct boundary conditions and interaction mechanisms. Cladding panels may exhibit both displacement-sensitive and acceleration-sensitive behaviour, depending on the governing failure mode. In-plane damage is primarily driven by relative displacements, while out-of-plane response is associated with inertial forces proportional to acceleration. In the present study, both aspects are considered; however, the classification adopted in Section 2 is based on the dominant in-plane response, in line with the assumptions of the simplified modelling framework.

Similarly, masonry infills may also develop distinct in-plane and out-of-plane failure mechanisms: the in-plane response is directly governed by drift demand, while the out-of-plane mechanism can be assessed through an overturning-type verification based on a code-oriented approach [39], namely by considering the PGA as the governing acceleration demand. In such a case, failure would correspond to the attainment of DS5 (Table A.4 - Appendix), which is associated with risk class C3. It is important to note that this simplified procedure does not account for the interaction between in-plane and out-of-plane response modes.

4.3. Linearization of $Sa(T_1)$-EDP curves

The Sa(T_1)-EDP curves derived from the multi-stripe analysis were linearized to obtain simplified relationships suitable for practical implementation of the proposed procedure (Eq. 3).

$$y = m \cdot S_a(T_1) \tag{3}$$

where Sa(T_1) is expressed in units of g.

A linear model passing through the origin is assumed, so that the response is fully defined by the slope coefficient (m), representing the sensitivity of the considered EDP to the seismic intensity. In agreement with the observations reported in Section 4.2, the linearization was performed by considering EDP values up to 0.2 g, corresponding to the quasi-elastic range of the structural response. This choice allows the exclusion of nonlinear effects observed at higher intensity levels, ensuring consistency with the assumptions underlying the simplified assessment framework. The resulting linear relationships, hereafter referred to as baseline curves, represent the initial, near-linear behaviour of the system. Fig. 12 illustrates examples of the linearised relationships for the roof drift ratio and the roof acceleration, while the corresponding slope coefficients (m) are reported in Table 9.

Table 9
Slope coefficients (m) of the linearised Sa(T₁)–EDP baseline relationships for the reference buildings.

Damage parameter/ Element	Pre-84	84-NS	84-S	2003-ND	2003-D
Roof displacement	7.053	4.724	7.700	8.856	8.012
Roof acceleration	24.118	27.243	17.742	17.415	18.409
Roof element	0.600	0.510	0.027	0.002	0.001
Horizontal cladding panel	0.203	0.136	0.234	0.246	0.200
Vertical cladding panel	0.963	0.660	0.572	0.662	0.577

5. Parametric analyses for the definition of correction factors

Parametric analyses were performed to quantify the influence of key building characteristics on the seismic response (Table 11), including the fundamental period of vibration, the presence of structural irregularities, cladding panels, masonry infills and overhead cranes. A reference building was adopted as a baseline configuration, corresponding to a taxonomy-based archetype used to derive relative modifications of the seismic response. This configuration is not intended to represent the full variability of the existing building stock, but rather to provide a consistent basis for the derivation of seismic demand models within each taxonomy class. Accordingly, the results of the parametric analyses are interpreted in a comparative manner, in terms of variations with respect to the reference configuration rather than absolute predictions. The selected geometry reflects recurrent structural features of Italian precast industrial buildings, such as typical span lengths, column heights, and connection layouts, as documented in previous studies [57].

The reference building used corresponds to the “84-S” typology, with the geometry shown in Fig. 3. This configuration reflects the construction period immediately following the update of the national seismic classification in 1984, which significantly expanded the number of municipalities classified as seismic. Buildings constructed in this period typically lacked modern capacity-design criteria, while friction connections characteristic of the pre-1984 era were progressively replaced by mechanical systems in seismic regions. For this reason, the “84-S” building is adopted as a representative intermediate configuration of the existing building stock.

It is assumed that the relative variations obtained from the parametric analyses can be extended, in a comparative sense, to the other taxonomy classes listed in Table 6. This assumption is consistent with the objective of defining correction factors applicable within the taxonomy-based framework. The structural system consists of columns with a square cross-section of 50 cm × 50 cm. The roof system is composed of double-T precast elements with a span of 2.5 m, mechanically connected to the beams by steel brackets anchored with M10 bolts.

Nonlinear multi-stripe analyses were performed using a nonlinear 3D

Table 10
Plastic hinge parameters for RC columns and forks used in the 3D parametric models.

	k_0 [kNm/rad]	k_1/k_0 [-]	M_y [kNm]	ϑ_p [rad]	ϑ_{pc} [rad]	ϑ_u [rad]	M_{res} [kNm]
Column	43,100	0.07	262.70	0.0174	0.0432	0.08	63.04
RC fork	5686	0.30	52.88	0.0067	0.0180	0.08	63.04

Table 11
Input parameters considered in the parametric analyses.

Parameter	Reference building	Values
Fundamental period	1.5s	1.0 s, 1.5 s, 1.8s
Presence of structural irregularities	No	No, Yes
Presence/Type of perimeter enclosures	No	No, Cladding panels, Masonry infills
Presence of an overhead crane	No	No, Yes

Table 12
Variation of slope coefficients as a function of the building fundamental period.

reference period [s]	1.0	1.5	1.8
Period range [s]	[0.8 - 1.2]	[1.2 - 1.6]	[1.6 - 2.0]
Roof displacement	−20 %	-	+30 %
Roof acceleration	-	-	-
Roof element	−20 %	-	+15 %
Horizontal cladding panel	−25 %	-	+40 %
Vertical cladding panel	−45 %	-	+95 %

model implemented in OpenSees [58], following the modelling strategy proposed by Bosio et al. [32]. While the full modelling details are not reproduced here for brevity, the key assumptions relevant to the present study are summarised below. Both structural and non-structural components are represented in the numerical model, allowing a detailed assessment of their seismic behaviour. The main nonlinear mechanisms considered include: plastic hinges at column bases and RC forks, hysteretic behaviour of roof-element-to-beam connections, nonlinear response of cladding-panel connections, and contact interactions between precast elements. Plastic hinges (moment–rotation) at column bases and RC forks are implemented using the Modified Ibarra-Medina-Krawinkler deterioration model [61], with parameters reported in Table 10.

Mechanical roof-element-to-beam connections are modelled through zero-length elements governed by an elastic–plastic hysteretic law, with secant stiffness and ultimate displacement equal to 1928 kN/m and 0.028 m, respectively. Contact interfaces between precast elements are represented by compression-only zero-length elements with an elastic stiffness of 1650 kN/m. Beam-to-column joints are modelled as simple hinges, neglecting their nonlinear contribution. Preliminary analyses indicate that the forces transmitted through these joints remain below the sliding activation threshold, which represents the most critical condition for friction-based connections. Therefore, including this additional nonlinearity would increase computational demand without producing a significant variation in the global response.

For the seismic input, 30 spectrum-compatible ground motions were selected and grouped into 10 increasing intensity levels, using the same procedure as for the definition of the $Sa(T_1)$- EDP baseline curves. The use of spectrum-compatible records ensures consistency with the target response spectrum and reduces bias related to the fundamental period of the structure. The selection of three records per intensity level is considered sufficient, as the objective of the parametric analyses is to evaluate relative variations of EDPs with respect to the reference configuration rather than absolute response dispersion.

Table 13
Mechanical parameters adopted for cladding panel connections.

	Connection [-]	Direction [-]	k_0 [kN/m]	F_y [kN]	Gap [m]
Horizontal panel	Top connection	In-plane	666	13	0.020
		Out-of-plane	25,000	28	-
	Bottom	In-plane	10,000	100	-
		Out-of-plane	1000	3	-
Vertical panel	Top connection	In-plane	571	13	0.035
		Out-of-plane	25,000	28	-

The first parametric study investigates the influence of the fundamental period of vibration. Variations in the fundamental period are introduced by modifying the building height. A stiffer configuration (H = 5 m, T ≈ 1.0 s) and a more flexible configuration (H = 10 m, T ≈ 1.8 s) are considered. Table 12 reports the variation of the slope coefficients relative to the reference building (T = 1.5 s). An increase in the fundamental period results in higher displacement demands, particularly for non-structural components. For T = 1.8 s, roof displacement increases by approximately 30 %, while the variation in EDPs reaches +95 % for vertical cladding panels. Conversely, for T = 1.0 s, a general reduction in EDPs is observed. These results highlight the strong sensitivity of non-structural components to changes in global stiffness and dynamic properties.

Further parametric analyses examine the influence of structural irregularities, cladding panels, masonry infills, and overhead cranes. Structural irregularities are introduced by adding an intermediate floor at approximately 4 m height in the first two spans, supported by additional columns (Fig. 3). Cladding panels are modelled considering both horizontal and vertical configurations, with connections represented using zero-length elements governed by elastic–perfectly plastic gap materials. This modelling approach enables capturing both in-plane and out-of-plane response of panel connections. The horizontal cladding panels are connected to the columns through bearing connections at the bottom and hammerhead anchors at the top, while vertical panels are connected to the beam at the top and anchored to the ground at the base. The behaviour of the panel-to-structure connections was modelled using zero-length elements, implemented through various parallel "Elastic–Perfectly Plastic Gap" materials (Table 13) allowing representation of both in-plane [15,64] and out-of-plane behaviour [65,66].

Masonry infills are represented using nonlinear compression-only springs calibrated with cracking and peak strength values of 260 kN and 324 kN, respectively [67]. Two configurations of infills were analysed: half-height and full-height infills. An overhead crane with a load capacity of 10 ton (self-weight of approximately 100 kN) was considered in the model. Its inclusion involved the modelling of rail beams with T-shaped cross sections (0.016 m^2) along the longitudinal direction, and a main transverse beam, assumed to be rigid. The crane was considered unloaded, and thus only its self-weight was considered. It is worth noting that the presence of the hoist mass on the crane might influence the building's structural response [68]. The crane is analysed in two positions (end-span and mid-span), and the envelope of the response is considered.

The results of the analyses (Table 14) show that structural irregularities have limited influence on roof displacement, roof acceleration and the response of the horizontal cladding panels, but significantly affect local response parameters, with increases of up to +60 % for roof elements. Cladding panels primarily affect roof acceleration (+20 %), while masonry infills significantly modify both roof acceleration (+45 %) and connection demand. The presence of an overhead crane reduces roof acceleration (−45 %) and slightly affects vertical cladding response. Overall, the results confirm that non-structural components and additional masses can significantly modify seismic demand, highlighting the importance of including these effects in simplified assessment procedures.

Table 14
Variation of slope coefficients associated with different structural and non-structural parameters.

Parameter	Irregularity	Cladding panels	Infill panels	Overhead crane
Roof displacement	-	-	−33 %	-
Roof acceleration	-	+20 %	+45 %	−45 %
Roof element	+60 %	-	-	-
Horizontal cladding panel	-	-	-	-
Vertical cladding panel	+15 %	-	-	+10 %

6. Validation and application of the proposed procedure

The developed procedure was validated through two complementary applications. First, the method was applied to a real industrial building damaged during the 2012 Emilia earthquakes, allowing a direct comparison between observed and predicted damage and thus assessing the reliability of the approach. Second, the procedure was implemented within the GEOSAFE platform to demonstrate its applicability in real-world decision-making contexts and its usability for non-expert users.

6.1. Case study: Validation against observed earthquake damage

To validate the proposed method through comparison with observed damage, a precast industrial building damaged during the May 2012 Emilia seismic sequence was selected as a representative case study [60]. The building is a single-storey precast industrial structure constructed in the 1970s in the province of Modena, Italy, with a rectangular plan (35 m × 11 m) and a height of 6.2 m. The external walls consist of masonry infill panels, and a mezzanine floor is present in the first bay, used for office space. The seismic sequence that struck the Emilia region in May 2012 was characterised by two mainshocks occurring on 20 and 29 May.

The observed damage to the columns primarily involved cracking at the base of the columns and around the ribbon window. The presence of the ribbon window introduced a vertical irregularity, leading to a short-column effect and increased damage concentration. The masonry infills contributed to an irregular structural response. At the roof level, excessive relative displacements led to the collapse of roof elements (Fig. 13-left), which in turn caused significant damage to the building contents (Fig. 13-right).

Subsequently, the developed procedure was applied following the steps described in Section 2. The seismic input was defined using the first mainshock (20 May 2012, MRN station, 5.9 Magnitude, epicentral distance 4.7 km, peak ground acceleration 0.264 g), as the proposed procedure does not account for cumulative damage from multiple seismic events.

Step 1. The building was constructed in the 1970s with a height of 6.2 m, therefore, the reference class "Pre-84" was selected. Relevant characteristics include structural irregularities (due to the mezzanine floor) and the presence of masonry infills.
Step 2. In the absence of information on retrofit interventions, the initially selected reference class is maintained.
Step 3. The fundamental period was estimated using Eq. 3 with $\alpha = 0.45$ and $H = 6.2$ m, resulting in $T_1 = 1.34$ s. Since this value falls within the range [1.2–1.6 s], no modification of the baseline curves is required.
Step 4. The baseline slope coefficients were updated to account for the specific characteristics of the building by applying multiplicative factors (Table 15).

Step 5. The spectral acceleration $Sa(T_1)$ was determined from the recorded response spectrum at the MRN station. To reduce

Table 16
EDP values for the case study building.

Considered EDP	EDP value
Drift at roof level	2.0 %
Roof acceleration	15.0 m/s^2
Beam-to-roof element relative displacement	0.413 m
Horizontal cladding panel-to-column relative displacement	0.087 m
Vertical cladding panel-to-beam relative displacement	0.476 m

Fig. 13. Observed damage patterns following the 29 May 2012 earthquake: collapse of roof elements (left) and consequent damage to building contents (right).

Table 15
Slope coefficient for the case study building.

Damage parameter	Reference slope coefficients	Multiplicative coefficients			Case study building
		Period class	Irregularity	Infill panels	
Roof displacement	7.053	1.0	1.0	0.67	4.726
Roof acceleration	24.118	1.0	1.0	1.45	34.971
Roof element	0.600	1.0	1.6	1.0	0.960
Horizontal cladding panel	0.203	1.0	1.0	1.0	0.203
Vertical cladding panel	0.963	1.0	1.15	1.0	1.107

Table 17
Exceedance probability of damage states for structural and non-structural elements.

	Column	Roof element	Masonry infill
DS1	0.776	1.000	1.000
DS2	0.619	1.000	0.997
DS3	0.467	1.000	0.951
DS4	0.027	1.000	0.581
DS5	-	1.000	-

uncertainty in the estimation of T_1, a preliminary modal analysis was performed using MidasGen [69], resulting in $T_1 = 1.24$ s and $Sa(T_1) = 0.43$ g. The EDP values, reported in Table 16, were then computed using the updated slope coefficients.

Step 6. Damage states were evaluated using the computed EDP values and fragility curves. For each component, the probability of exceeding each damage state was calculated. An example is reported in Table 17.

Step 7. The predicted risk classes were compared with observed damage (Table 18). The results show good agreement for structural elements, while a conservative estimate is observed for masonry infills. This behaviour reflects the simplified nature of the method, which prioritises robustness over exact prediction of damage.

The method identifies significant risk classes for both structural and non-structural components, with risk classes of C3 and C5 for columns and roof elements, respectively, and C2-C3 for infill panels. In the absence of detailed information on building contents at the time of the earthquake, a representative set of non-structural and content elements was considered.

To assess the sensitivity of the proposed method, additional analyses were performed by scaling the acceleration spectrum of the 2012 Emilia earthquake to lower intensity levels, corresponding to $Sa(T_1)$ values of 0.2 g and 0.067 g. These values represent seismic scenarios associated with the Life Safety (LS) and Damage Limit (DL) states for the site. Table 19 compares the exceedance probabilities of selected damage states for key elements while Table 20 reports the corresponding risk classes. The results show a clear reduction in damage levels under lower

Table 18
Comparison between observed damage and predicted risk classes.

	Observed damage states	Risk class	
		Observed	Estimated
Columns	Limited damage (DS2). 	C3	C3
Roof elements	Collapse (DS5). 	C5	C5
Masonry infills	Diagonal cracking in infill panels (DS2). 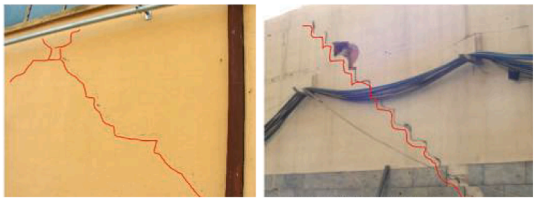	C2	C3

Table 19
Exceedance probabilities for different seismic intensity levels (Emilia, LS, DL).

	Column			Roof element			Masonry infill		
	Emilia	LS	DL	Emilia	LS	DL	Emilia	LS	DL
DS1	0.776	0.124	0.000	1.000	1.000	1.000	1.000	0.999	0.861
DS2	0.619	0.054	0.000	1.000	1.000	1.000	0.997	0.909	0.245
DS3	0.467	0.023	0.000	1.000	1.000	0.998	0.951	0.396	0.001
DS4	0.027	0.000	0.000	1.000	1.000	0.882	0.581	0.035	0.000
DS5	-	-	-	1.000	0.998	0.569	-	-	-

Table 20
Comparison of risk classes for structural, non-structural, and content components.

	Elements	Emilia 2012	LS	DL
Structural elements	Columns	C3	C0	C0
	Roof elements	C5	C5	C5
	Masonry infills	C3	C1	C1
	Vertical cladding panels	C3	C3	C3
	Horizontal cladding panel	C3	C2	C0
Non-structural elements	Sealant	C2	C1	C0
	Windows	C3	C1	C0
	Drywall partitions	C2	C2	C1
	Internal doors	C2	C2	C2
	Storage racks	C3	C3	C0
	Hydraulic elevator	C3	C3	C0
	Electric elevator	C3	C3	C0
	Refrigeration unit	C2	C2	C0
	Distribution panel	C0	C0	C0
Contents	Generator	C3	C0	C0
	Low-voltage electrical panel	C2	C0	C0
	Control centre	C0	C0	C0
	Compressor	C2	C0	C0
	Air handling unit	C2	C0	C0
	Cooling towers	C2	C0	C0
	Overhead crane	C3	C3	C0

seismic intensities, with most components exhibiting limited or negligible damage in LS and DL conditions. This indicates that the building would have maintained adequate performance under moderate seismic events. However, certain elements, such as roof components and vertical cladding panels, remain highly vulnerable, highlighting intrinsic weaknesses in their design.

6.2. *Implementation and application within the GEOSAFE platform*

The proposed methodology was implemented within the GEOSAFE platform [70,71], an online tool developed by ANIA SAFE to support seismic risk assessment and decision-making. The implementation enables automated retrieval of site-specific seismic input, application of the taxonomy-based classification framework, and rapid computation of risk classes. The workflow mirrors the proposed methodology: the user selects the building location, inputs basic information (construction year, height), and optionally provides details on retrofitting, irregularities, cladding, and equipment. The platform generates a structured report including risk classification results presented through a colour-coded system, facilitating interpretation.

The output (Fig. 14) highlights the relative vulnerability of different components, supporting rapid identification of critical elements and prioritisation of mitigation measures.

7. Conclusions

In this paper, a taxonomy-based procedure for the seismic risk classification of single-storey precast industrial buildings has been presented, explicitly accounting for structural, non-structural, and content-related components. The method incorporates key building characteristics, including construction period, structural irregularities, cladding systems, and the presence of overhead cranes, within a simplified yet mechanically informed assessment framework.

A set of risk classes was defined by grouping seismic intensity levels derived from the macroseismic scale, and these classes were assigned to individual components based on the correspondence between global damage scenarios and component-level damage states. Within this framework, a taxonomy of precast industrial buildings in Italy was established, identifying five reference classes associated with different construction periods and seismic design practices. A complementary procedure was also introduced to account for retrofit interventions when defining the appropriate reference class.

The seismic response of the buildings was evaluated using a combination of simplified 2D numerical models and refined 3D models. The 2D models were employed to derive baseline $Sa(T_1)$–EDP relationships for each taxonomy class, while parametric analyses based on 3D models were used to define correction factors accounting for building-specific features. Damage assessment was performed through component-specific fragility functions, with reference to FEMA P-58 for non-structural and content elements.

The proposed procedure was validated through application to a real industrial building damaged during the 2012 Emilia earthquake. A good agreement was observed between predicted and observed damage for the main structural elements, while a slightly conservative estimation was obtained for non-structural components. This behaviour is consistent with the simplified nature of the method, which is intended for rapid assessment and prioritisation purposes rather than for detailed loss

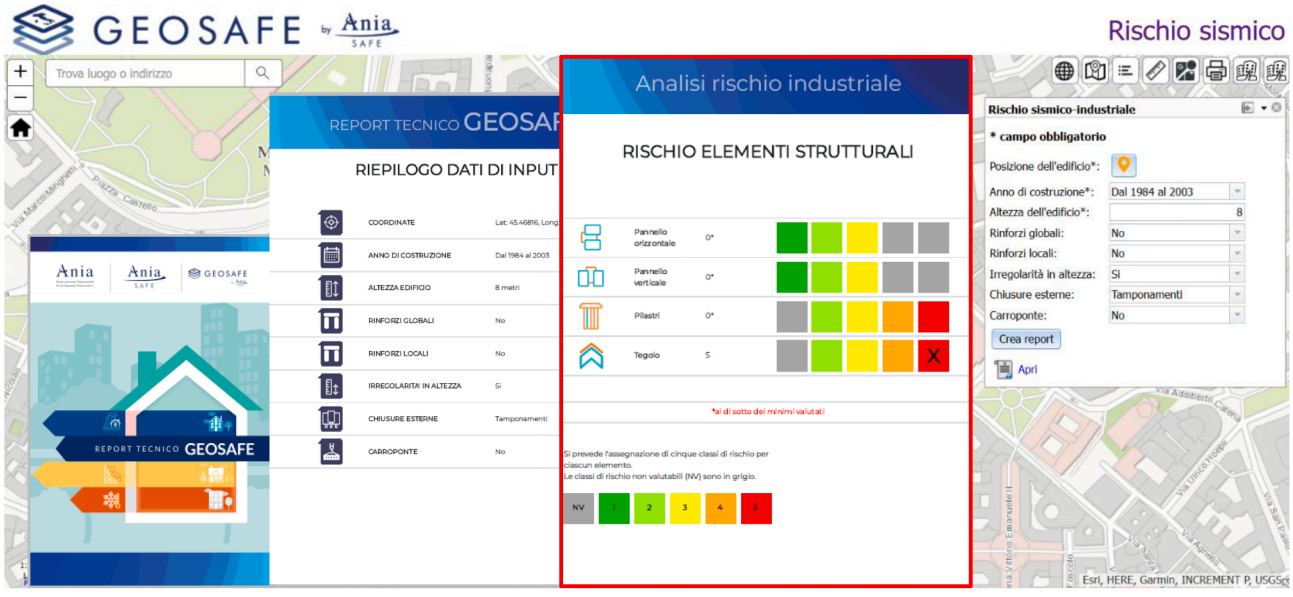

Fig. 14. Example of GEOSAFE output showing the component-based vulnerability matrix for a precast industrial building.

estimation. The sensitivity analyses performed under reduced seismic intensities demonstrated the capability of the method to differentiate between different performance levels and risk scenarios.

The methodology was further implemented within the GEOSAFE platform, enabling automated application and facilitating its use by non-expert users. This implementation demonstrates the potential of the proposed approach for large-scale screening, risk prioritisation, and preliminary decision-making processes.

It is important to note that the proposed procedure primarily addresses the vulnerability component of seismic risk, while exposure and consequence modelling are only partially represented. Future developments may focus on integrating economic loss models and expanding the calibration of fragility functions, particularly for non-structural and content-related components, to enhance the accuracy and applicability of the method.

Data availability

Data and material related to the paper are available upon request to the authors. Closed-source software was employed for the development of the work contained in the paper.

CRediT authorship contribution statement

Marius Eteme Minkada: Writing – original draft, Formal analysis, Data curation, Visualization. **Andrea Belleri:** Writing – review & editing, Validation, Methodology, Conceptualization, Supervision. **Marco Bosio:** Writing – review & editing, Validation, Formal analysis, Data curation. **Luca Rota:** Writing – review & editing, Visualization, Formal analysis.

Declaration of competing interest

Please find the declaration of Interest Statement of the manuscript entitled “A Taxonomy-Based Rapid Assessment Procedure for Seismic Risk Classification of Single-Storey Precast RC Buildings” by Marius Eteme Minkada et al.

The authors declare that they have no known competing financial interests or personal relationships that could have appeared to influence the work reported in this paper.

Acknowledgements

The research presented in this paper was carried out within the framework of a project supported by ANIA Safe, Milan, Italy. The authors gratefully acknowledge the financial support provided. The views and conclusions expressed herein are those of the authors and do not necessarily reflect the official position of the people and organization acknowledged.

Appendix A. Description of damage states and risk class assignment criteria

This appendix provides the qualitative definitions of the damage states adopted for structural, non-structural, and content-related components, together with the criteria used for mapping damage states to risk classes. The adopted definitions are based on available literature [32,33] and are reported in Tables A.1–A.6. For structural elements, damage states range from minor cracking to severe damage and collapse, while for non-structural components they describe progressive degradation from initial detachment and cracking to extensive damage and failure, accounting for both in-plane and out-of-plane mechanisms where relevant.

For content-related components, it should be noted that fragility models available in FEMA P-58 typically define a single damage state (DS1), generally associated with loss of operability. In this study, this representation is extended for selected components to better capture different levels of functional and structural damage. Two damage states (DS1 and DS2) are defined for storage racks and overhead cranes, distinguishing between loss of functionality and structural damage or instability. This extension enables a more refined representation of the consequences associated with content damage, which is particularly relevant in industrial buildings.

Table A.1
Assignment of seismic risk classes for the column.

Element	Damage state	Description	Risk class
Column	DS1	Micro-cracks appear primarily in the concrete cover; the section at the base of the column remains within its elastic range.	C2
	DS2	Limited damage: small cracks may develop, typically in concrete cover, without significant loss of strength or stiffness.	C3
	DS3	Extensive cracking, severe spalling, and exposure of reinforcement; noticeable reduction in stiffness and strength.	C4
	DS4	Collapse: extensive damage characterized by a loss of stiffness and a 50 % reduction in load-bearing capacity.	C5

Table A.2
Assignment of seismic classes for the roof element.

Element	Damage state	Description	Risk class
Roof element	DS1	Yielding of connections or activation of sliding	C2
	DS2	Relative sliding of 1 cm	C2
	DS3	Relative sliding of 2 cm	C3
	DS4	Relative sliding of 4 cm	C4
	DS5	Collapse: relative displacement greater than 6 cm	C5

Table A.3
Assignment of seismic risk classes for the sealant, vertical and horizontal cladding panels.

Element	Damage state	Description	Risk class
Sealant	DS1	Micro-cracks visible on the surface, indicating initial deterioration	C1
	DS2	Collapse with loss of adhesion and functionality	C2
Vertical panel	DS1	Micro-cracks on the sealant	-
	DS2	Sealant failure	-
	DS3	Yielding of connections	C2
	DS4	Panel collapse	C3
Horizontal panel	DS1	Beginning of sealant cracking	-
	DS2	Sealant failure	-
	DS3	Yielding of connections	C2
	DS4	Panel collapse	C3

Table A.4
Assignment of seismic risk classes for the masonry infills.

Element	Damage state	Description	Risk class
Brick masonry infills	DS1	Separation of the infill panel from the reinforced concrete frame at the underside of the beam and along the height of the columns, with minor cracks in the masonry	C1
	DS2	Damage to the infill panel with the onset of diagonal cracking.	C1
	DS3	Extensive detachment of plaster; significant sliding at mortar joints and further development of cracks in the panel; crushing of bricks; if there are openings in the infill, the window remains undamaged.	C2
	DS4	A large area of the masonry panel is affected by crushing/chipping of blocks/bricks, and the panel is close to collapse; if there are openings in the infill, the window is damaged.	C3
	DS5	Collapse due to in-plane mechanisms or out-of-plane overturning.	-

Table A.5
Assignment of seismic risk classes for the windows.

Element	Damage state	Description	Risk class
Windows	DS1	Frame-to-glass contact and minor perimeter crack on the glass	C1
	DS2	Sealant failure	C2
	DS3	Glass shift and gasket detachment	C2
	DS4	Visible cracks on the glass	C2
	DS5	Large cracks and glass detachment	C3

Table A.6
Assignment of seismic risk classes for internal drywall partitions and internal doors.

Element	Damage state	Description	Risk class
Internal drywall partitions	DS1	Initial visible damage consisting of minor cracks (does not require panel replacement)	C1
	DS2	Significant cracks and crushings in the drywall panels	C2
	DS3	Severe damage to the panel and frame (requiring partition replacement).	C2
Internal doors	DS1	The door gets stuck and cannot be opened	C2
	DS2	Damage to the door lock and/or hinges	C2

References

[1] ISO 31010. Risk management - Risk assessment techniques. International Organization for Standardization; 2009.
[2] A. Anelli, S. Santa-Cruz, M. Vona, N. Tarque, M. Laterza, An innovative methodology for the seismic risk mitigation on large territorial scale, in: World Engineering Conference on Disaster Risk Reduction, Lima, 2016.
[3] F. Braga, M. Dolce, D. Liberatore, A statistical study on damaged buildings and an ensuing review of the MSK-76 scale, in: 7th European Conference on Earthquake Engineering, 1982.
[4] Rossetto T, Elnashai A. Derivation of vulnerability functions for European-type RC structures based on observational data. Eng Struct 2003;25:1241–63. https://doi.org/10.1016/S0141-0296(03)00060-9.
[5] P. Angeletti, A. Bellina, E. Guagenti Grandori, A. Moretti, V. Petrini, Comparison between vulnerability assessment and damage index: some results, in: 9th World Conference on Earthquake Engineering, Kyoto, 1988.
[6] Harirchian E, Lahmer T, Buddhiraju S, Mohammad K, Mosavi A. Earthquake safety assessment of buildings through rapid visual screening. Buildings 2020;10:51. https://doi.org/10.3390/buildings10030051.
[7] Petruzzelli F, Iervolino I. NODE: a large-scale seismic risk prioritization tool for Italy based on nominal structural performance. Bull Earthq Eng 2021;19:2763–96. https://doi.org/10.1007/s10518-021-01133-9.
[8] S. Menoni, V. Petrini, G. Zonno, Seismic risk evaluation through integrated use of information systems and artificial intelligence techniques, 1997.
[9] Grant DN, Bommer JJ, Pinho R, Calvi GM, Goretti A. A prioritization scheme for seismic intervention in school buildings in Italy. Earthq Spectra 2007;23:291–314. https://doi.org/10.1193/1.2431396.
[10] H. Crowley, M. Colombi, G.M. Calvi, R. Pinho, F. Meroni, A. Cassera, Application of a prioritisation scheme for seismic intervention in school buildings in Italy, in: 14th World Conference on Earthquake Engineering, Beijing, 2008.
[11] Lagomarsino S, Giovinazzi S. Macroseismic and mechanical models for the vulnerability and damage assessment of current buildings. Bull Earthq Eng 2006;4:415–43. https://doi.org/10.1007/s10518-006-9024-z.

[12] Vona M, Anelli A, Tufaro T, Harabaglia P, Mori F, Manganelli B. Seismic resilience-based strategies for prioritization of interventions on a subregional area. Bull Earthq Eng 2024;23:113–47. https://doi.org/10.1007/s10518-023-01709-0.
[13] Toniolo G, Colombo A. Precast concrete structures: the lessons learned from the L'Aquila earthquake. Struct Concr 2012;13:73–83. https://doi.org/10.1002/suco.201100014.
[14] Brunesi E, Nascimbene R, Bolognini D, Belotti D. Experimental investigation of the cyclic response of reinforced precast concrete framed structures. PCI J 2015;60:57–79.
[15] Belleri A, Torquati M, Marini A, Riva P. Horizontal cladding panels: in-plane seismic performance in precast concrete buildings. Bull Earthq Eng 2016;14:1103–29. https://doi.org/10.1007/s10518-015-9777-1.
[16] Belleri A. Displacement-based design for precast concrete frames with non-emulative connections. Eng Struct 2017;141:228–40. https://doi.org/10.1016/j.engstruct.2017.02.047.
[17] Dal Lago B, Ferrara L. Efficacy of roof-to-beam mechanical connections on the diaphragm behaviour of precast decks with spaced roof elements. Eng Struct 2018;176:681–96. https://doi.org/10.1016/j.engstruct.2018.09.044.
[18] Torquati M, Belleri A, Riva P. Displacement-based seismic assessment for precast concrete frames with non-emulative connections. J Earthq Eng 2020;24:1624–51. https://doi.org/10.1080/13632469.2018.1555660.
[19] Ercolino M, Bellotti D, Magliulo G, Nascimbene R. Vulnerability analysis of industrial RC precast buildings designed according to modern seismic codes. Eng Struct 2018;158:67–78. https://doi.org/10.1016/j.engstruct.2017.12.028.
[20] I. Iervolino, A. Spillatura, P. Bazzurro, RINTC e project: risk assessment of existing residential reinforced concrete buildings in Italy, in: 7th ECCOMAS Thematic Conference on Computational Methods in Structural Dynamics and Earthquake Engineering, 2019.
[21] Bressanelli ME, Bellotti D, Belleri A, Cavalieri F, Riva P, Nascimbene R. Influence of modelling assumptions on the seismic risk of industrial precast concrete structures. Front Built Environ 2021;7:629956. https://doi.org/10.3389/fbuil.2021.629956.
[22] Belleri A, Dal Lago B, Rodrigues H. Advances in seismic performance and risk estimation of precast concrete buildings. Front Built Environ 2021;7. https://doi.org/10.3389/fbuil.2021.640710.
[23] DPC. Indicazioni alle componenti ed alle strutture operative del servizio nazionale di protezione civile per l'aggiornamento delle pianificazioni di protezione civile per il rischio maremoto. Gazzetta Ufficiale; 2018.
[24] Magliulo G, Fabbrocino G, Manfredi G. Seismic assessment of existing precast industrial buildings using static and dynamic nonlinear analyses. Eng Struct 2008;30:2580–8. https://doi.org/10.1016/j.engstruct.2008.01.018.
[25] Senel SM, Kayhan AH. Fragility-based damage assessment in existing precast industrial buildings: a case study for Turkey. Struct Eng Mech 2010;11:39–58. https://doi.org/10.12989/sem.2010.36.4.451.
[26] Palanci M, Senel SM, Kalkan A. Assessment of one-story existing precast industrial buildings in Turkey based on fragility curves. Bull Earthq Eng 2017;15:271–89. https://doi.org/10.1007/s10518-016-9970-4.
[27] Bosio M, Di Salvatore C, Bellotti D, Capacci L, Belleri A, Piccolo V, Cavalieri F, Dal Lago B, Riva P, Magliulo G, Nascimbene R, Biondini F. Modelling and seismic response analysis of non-residential single-storey existing precast buildings in Italy. J Earthq Eng 2023;27:1047–68. https://doi.org/10.1080/13632469.2021.1953114.
[28] Magliulo G, Bellotti M, Cimmino M, Nascimbene R. Modelling and seismic response analysis of RC precast Italian code-conforming buildings. J Earthq Eng 2018:40–67. https://doi.org/10.1080/13632469.2017.1297264.
[29] Magliulo G, Di Salvatore C, Ercolino M. Modeling of the beam-to-column dowel connection for a single-story RC precast building. Front Built Environ 2021;7:627546. https://doi.org/10.3389/fbuil.2021.627546.
[30] FEMA. HAZUS-MH MR4 technical manual. Washington, D.C.: Federal Emergency Management Agency; 2003. Available at: https://www.fema.gov/plan/prevent/hazus/hz_manuals.shtm.
[31] Brzev S, Scawthorn C, Charleson AW, Allen L, Greene M, Jaiswal K, Silva V. GEM Building Taxonomy Version 2.0. GEM technical report 2013-02. Pavia: GEM Foundation; 2013. https://doi.org/10.13117/GEM.EXP-MOD.TR2013.02.
[32] Bressanelli ME, Bellotti D, Belleri A, Cavalieri F, Riva P, Nascimbene R. Seismic risk and finite element modelling influence of an existing one-storey precast industrial building. J Earthq Eng 2023;24:1363–2469. https://doi.org/10.1080/13632469.2020.1864441.
[33] FEMA. FEMA P-58-3: seismic performance assessment of buildings, volume 3 – supporting electronic materials. Washington, D.C.: Federal Emergency Management Agency; 2012.
[34] Grünthal G. European macroseismic scale 1998, cahiers du centre européen de géodynamique et de séismologie 1998;15.
[35] Decreto legge n. 1526 del 5 novembre 1916, testo unico delle disposizioni legislative emanate in dipendenza del terremoto del 28 dicembre 1908. Gazzetta Ufficiale; 1916. n. 247 del 17 novembre 1916.
[36] Decreto Regio. Norme tecniche ed igieniche obbligatorie per le riparazioni, ricostruzioni e nuove costruzioni degli edifici pubblici e privati nei luoghi colpiti dal terremoto del 28 dicembre 1908 e da altri precedenti elencati nel R.D. 15 aprile 1909. Gazzetta Ufficiale; 1909. n. 95 del 22 aprile 1909.
[37] Decreto Regio. n. 705 del 3 aprile 1926, modificazioni alle norme tecniche ed igieniche di edilizia obbligatorie per le località colpite da terremoti. Gazzetta Ufficiale; 1926. n. 102 del 3 maggio 1926.
[38] OPCM. Primi elementi in materia di criteri generali per la classificazione del territorio nazionale e di normative tecniche. Gazzetta Ufficiale; 2003. n. 3274 del 20 marzo 2003.
[39] NTC. Decreto ministeriale 14 gennaio 2008, norme tecniche per le costruzioni. Gazzetta UfficialeGazzetta Ufficiale; 2008. n. 29 del 4 febbraio 2008; Circolare applicativa n. 617 C.S.LL.PP.n. 47 del 26 febbraio 2009.
[40] NTC. Norme tecniche per le costruzioni, decreto ministeriale 17 gennaio 2018. Gazzetta Ufficiale; 2018.
[41] Decreto Ministeriale. n. 108 del 24 gennaio 1986, norme tecniche relative alle costruzioni antisismiche. Gazzetta Ufficiale; 1986.
[42] Decreto Ministeriale. 3 dicembre 1987, norme tecniche per la progettazione, esecuzione e collaudo delle costruzioni prefabbricate. Gazzetta Ufficiale; 1987. n. 106 del 7 maggio 1988.
[43] Magliulo G, Ercolino M, Petrone C, Coppola O, Manfredi G. The Emilia earthquake: seismic performance of precast reinforced concrete buildings. Earthq Spectra 2014;30:891–912. https://doi.org/10.1193/022813EQS050M.
[44] Belleri A, Brunesi E, Nascimbene R, Pagani M, Riva P. Seismic performance of precast industrial facilities following major earthquakes in the Italian territory. J Perform Constr Facil 2015;29:04014133. https://doi.org/10.1061/(ASCE)CF.1943-5509.0000623.
[45] Demartino C, Monti G, Vanzi I. Seismic loss of support conditions of frictional beam-to-column connections. Struct Eng Mech 2017;61:527–38. https://doi.org/10.12989/sem.2017.61.4.527.
[46] Di Trapani F, Ferro GA, Malavisi M. Definition of inelastic displacement demand spectra for precast industrial facilities with friction and fixed beam-to-column joints. Soil Dyn Earthq Eng 2020;128:105865. https://doi.org/10.1016/j.soildyn.2019.105865.
[47] Labò S, Eteme Minkada M, Marini A, Belleri A. Loss of support assessment for precast portal frames with friction connections and masonry infills. Bull Earthq Eng 2022;20:7983–8009. https://doi.org/10.1007/s10518-022-01487-3.
[48] G. Toniolo, SAFECAST Project: european research on seismic behaviour of the connections of precast structures, in: 15th World Conference on Earthquake Engineering, Lisbon, 2012.
[49] Zoubek B, Fischinger M, Isaković T. Estimation of the capacity of beam-to-column dowel connections in precast industrial buildings. Bull Earthq Eng 2014;13:2145–68. https://doi.org/10.1007/s10518-014-9682-4.
[50] B. Zoubek, M. Fischinger, T. Isaković, Influence of beam-to-column dowel connection detailing on the seismic fragility of precast industrial buildings, in: 16th World Conference on Earthquake Engineering, Santiago, Chile, 2017.
[51] Biondini F, Toniolo G. Probabilistic calibration and experimental validation of the seismic performance of precast structures. Bull Earthq Eng 2009;13:426–62. https://doi.org/10.1007/s10518-008-9080-3.
[52] Biondini F, Dal Lago B, Toniolo G. Role of wall panel connections on the seismic performance of precast structures. Bull Earthq Eng 2013;11:1061–81. https://doi.org/10.1007/s10518-012-9410-3.
[53] Minghini F, Tullini N. Seismic retrofitting solutions for precast RC industrial buildings struck by the 2012 earthquakes in Northern Italy. Front Built Environ 2021;7. https://doi.org/10.3389/fbuil.2021.642046.
[54] M. Eteme Minkada, M. Bosio, A. Belleri, P. Riva, Influence of cladding panels retrofit on the seismic risk of an existing precast building, in: 9th ECCOMAS Thematic Conference on Computational Methods in Structural Dynamics and Earthquake Engineering, Athens, 2023.
[55] Silva V, Brzev S, Scawthorn C, Yepes C, Dabbeek J, Crowley H. A building classification system for multi-hazard risk assessment. Int J Disaster Risk Reduct 2022;70:102772. https://doi.org/10.1016/j.ijdrr.2021.102772.
[56] Magliulo G, Ercolino M, Manfredi G. Influence of cladding panels on the first period of one-story precast buildings. Bull Earthq Eng 2015;13:1531–55. https://doi.org/10.1007/s10518-014-9657-2.
[57] Bonfanti C, Carabellese A, Toniolo G. Strutture prefabbricate: catalogo delle tipologie esistenti. ReLUIS–ASSOBETON; 2008.
[58] McKenna F, Fenves GL, Scott MH. Open system for earthquake engineering simulation. University of California, Berkeley; 2000.
[59] M. Eteme Minkada, S. Labò, A. Marini, A. Belleri, Preliminary considerations on the loss of support for precast beam elements, in: 8th International Conference on Computational Methods in Structural Dynamics and Earthquake Engineering (COMPDYN), 2021.
[60] Angiolilli M, Eteme Minkada M, Di Domenico M, Cattari S, Belleri A, Verderame GM. Comparing the observed and numerically simulated seismic damage: a unified procedure for unreinforced masonry and reinforced concrete buildings. J Earthq Eng 2022:1–37. https://doi.org/10.1080/13632469.2022.2063534.
[61] Ibarra L, Medina R, Krawinkler H. Hysteretic models that incorporate strength and stiffness deterioration. Earthq Eng Struct Dyn 2005;34:1489–511. https://doi.org/10.1002/eqe.495.
[62] Meletti C, Montaldo V, Stucchi M, Martinelli F. Database della pericolosità sismica MPS04. Istituto Nazionale di Geofisica e Vulcanologia; 2006.
[63] Iervolino I, Galasso C, Cosenza E. REXEL: computer aided record selection for code-based seismic structural analysis. Bull Earthq Eng 2009;8:339–62. https://doi.org/10.1007/s10518-009-9146-1.
[64] Foti F, Dal Lago B, Martinelli L. On the coupled dynamics of vertical cladding panels and industrial frame structures subject to out-of-plane seismic loading. Eng Struct 2023;296:116909. https://doi.org/10.1016/j.engstruct.2023.116909.
[65] Zoubek B, Fischinger M, Isaković T. Cyclic response of hammer-head strap cladding-to-structure connections used in RC precast buildings. Eng Struct 2016;119:135–48. https://doi.org/10.1016/j.engstruct.2016.04.002.
[66] Belleri A, Cornali F, Passoni C, Marini A, Riva P. Evaluation of out-of-plane seismic performance of column-to-column precast concrete cladding panels in one-storey industrial buildings. Earthq Eng Struct Dyn 2018;47:397–417. https://doi.org/10.1002/eqe.2956.

[67] Colangelo F. Pseudo-dynamic seismic response of reinforced concrete frames infilled with non-structural brick masonry. Earthq Eng Struct Dyn 2005;34:1219–41. https://doi.org/10.1002/eqe.474.
[68] Belleri A, Labò S, Marini A, Riva P. The influence of overhead cranes on the seismic performance of industrial buildings. Front Built Environ 2017;3:64. https://doi.org/10.3389/fbuil.2017.00064.
[69] MIDAS, MIDASGen-Analysis manual, 2020.
[70] Ania SAFE, GEOSAFE – Sistema informative geografico a support della valutazione del rischio.accessed 2026. https://www.geosafe.ania.it/.
[71] Eteme Minkada M, Belleri A, Bosio M, Rota L, Riva P, Pasetti N, Ranghetti M. Seismic risk assessment of precast industrial buildings in Italy by the GEOSAFE platform. Procedia Struct Integr 2026;78:177–84. https://doi.org/10.1016/j.prostr.2025.12.023.